Climate Dynamics 55: 3431–3444 (2020)

Authors
Oliver Meseguer-Ruiz*, Paulina I. Ponce-Philimon, Alexis Baltazar, Jose A. Guijarro, Roberto Serrano-Notivoli, Jorge Olcina Cantos, Javier Martín-Vide, Pablo Sarricolea

Title
Synoptic attributions of extreme precipitation in the Atacama Desert (Chile)

Affiliations
Oliver Meseguer-Ruiz
Departamento de Ciencias Históricas y Geográficas, Universidad de Tarapacá
2222, 18 de Septiembre, Arica, Chile
omeseguer@academicos.uta.cl
ORCID: 0000-0002-2222-6137
Paulina I. Ponce-Philimon
Departamento de Ciencias Históricas y Geográficas, Universidad de Tarapacá
2222, 18 de Septiembre, Arica, Chile
Alexis Baltazar
Departamento de Ciencias Históricas y Geográficas, Universidad de Tarapacá
2222, 18 de Septiembre, Arica, Chile
Jose A. Guijarro
State Meteorological Agency (AEMET)
Balearic Islands Office, Palma, Spain
Roberto Serrano-Notivoli
Estación Experimental de Aula Dei, Consejo Superior de Investigaciones Científicas (EEAD-CSIC)
Avda. Montañana 1005, Zaragoza, Spain
Jorge Olcina Cantos
Instituto Interuniversitario de Geografía, Universidad de Alicante
Edificio de Institutos Universitarios, Apartado de Correos 99, 03080 Alicante, Spain
Javier Martín-Vide
Departamento de Geografía, Universidad de Barcelona
Montalegre 6-8, 08001 Barcelona, Spain
Pablo Sarricolea
Departamento de Geografía, Universidad de Chile
Portugal 84, Torre Chica, Santiago, Chile

* Corresponding author

Abstract
Northern Chile is a region characterised by an extremely dry climate; however, there is a brief rainy season from December to March (austral summer), mainly above 3000 m a.s.l. It is interesting to consider where the humid air masses that generate such rain come from. For this purpose, daily precipitation data from 161 meteorological stations located in this area (18ºS to 19ºS) were considered, and four clusters formed by k-means clustering. For each cluster, days of extreme precipitation (above 90th percentile) were selected to obtain flow strength (F), direction (D), and vorticity (Z) for each event according to the Jenkinson and Collison (JC) method. The back trajectory, for the previous 72 h, of air masses affecting the centroid of each cluster was determined by means of the Hybrid Single-Particle Lagrangian Integrated Trajectory (HYSPLIT) model. The analyses were carried out at sea level (1013 hPa) and in the middle (500 hPa) and upper (250 hPa) troposphere. Surface circulation was not a determining factor in the occurrence of extreme events, but it did influence circulation at 500 and 250 hPa. For stations located in the northern Altiplano, moisture advection from the Amazon basin is evident due to the configuration of the Bolivian high—an upper level anticyclone that develops over the Bolivian Altiplano during austral summer. For stations located in the southern part of the study area, the main source of moisture is the Pacific Ocean, and the weather is related to the arrival of frontal systems and to the configuration of cut-off low pressure systems in the mid-troposphere.

Keywords
Back trajectory, extreme precipitation, Jenkinson and Collison method, HYSPLIT model, Northern Chile

1. Introduction

The Atacama Desert is one of the most arid regions in the world, covering a vast area including parts of Chile, Argentina, Bolivia, and Peru. In addition to severe aridity, this region is characterised by complex orography. This is the case in Northern Chile (17ºS to 29ºS), a region with an extreme elevation gradient between the Pacific Ocean on the west and the ranges of the Altiplano and Andes mountains (Fig. 1, Sarricolea et al. 2017a). Arid regions, such as the one studied here, are more sensitive to climate change (Donat et al. 2016; Shukla et al. 2019). Coastal deserts such as the Atacama are also affected by cold sea currents (in this case, the Humboldt Current) contribute to the scarcity and irregularity of rainfall (Bombi 2018; Rohde et al. 2019). In addition, rainfall projections in arid regions contain a high degree of uncertainty at regional and local scales (Williams 2017; Baez-Villanueva et al. 2018). This lack of consistency is characteristic of extremely high dry areas located at low latitudes (Kirtman et al. 2013), such as that found in northern Chile (Castino et al. 2017).

For example, rainfall exhibits irregularity at different time scales, from daily to multidecadal (Falvey and Garreaud 2005; Valdés-Pineda et al. 2018; Kock et al. 2020), that correspond to different mechanisms and the influence of the Andes mountains, which divide northern Chile into a coastal area in the west—under the influence of cold dry winds from the Pacific Ocean (Houston and Hartley 2003)—and a continental area in the east—influenced by warm wet easterly winds blowing from the Amazon basin (Garreaud 2009). The Andes mountains have a significant influence on moisture transport as well (Insel et al. 2010).

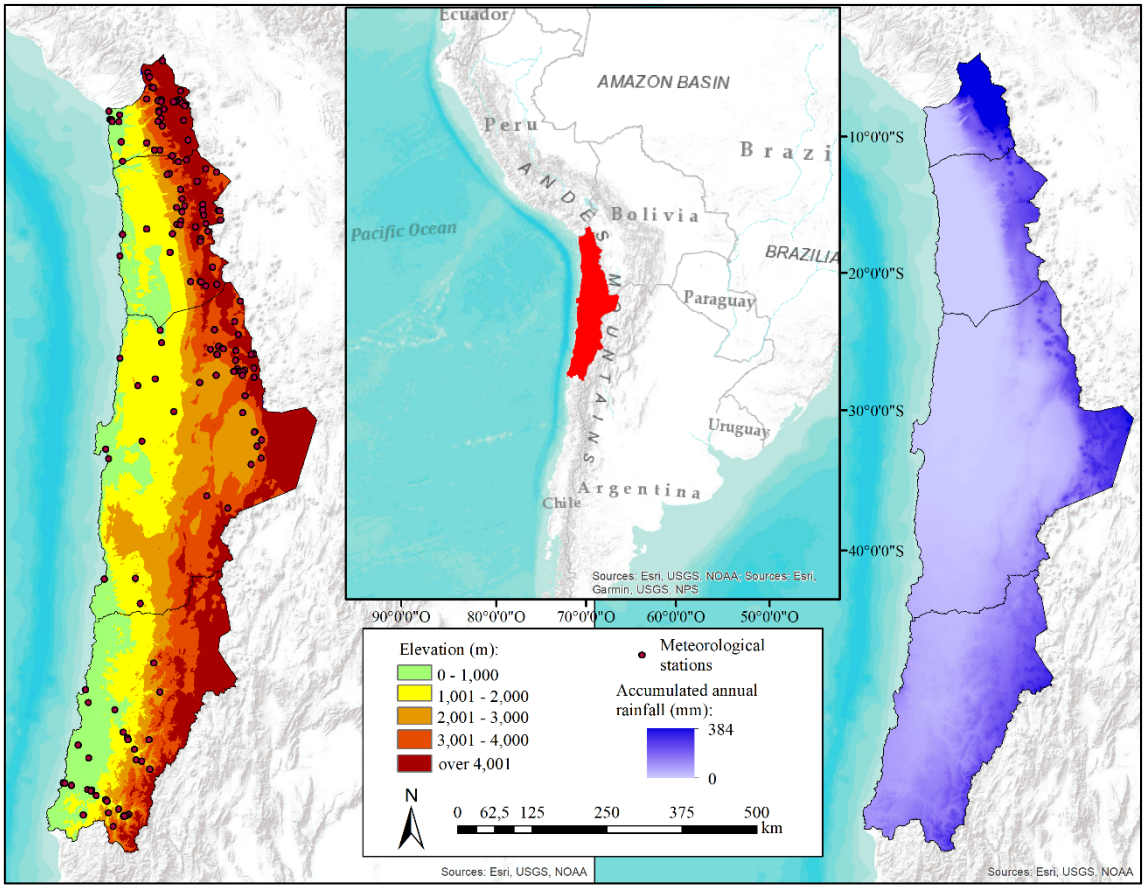

Figure 1. Map showing the topography of the study area and locations of the 161 meteorological stations employed (left), and the spatial distribution of mean annual precipitation (right) between 1950 and 2000 (Pliscoff et al. 2014).

The El Niño-Southern Oscillation is one of the mechanisms modulating seasonal and interannual variability in precipitation in northern Chile (Garreaud and Aceituno 2001; Valdés-Pineda et al. 2015). The frequency of El Niño and La Niña events may change under various global warming scenarios as will its influence on the irregularity of precipitation (Marjani et al. 2019). On an intraseasonal scale, precipitation responds to the configuration of the Bolivian high, an upper-level anticyclone (250 hPa, Meseguer-Ruiz et al. 2019a), which develops during the austral summer over the Bolivian Altiplano, a high plateau region of the Central Andes. The proximity of the Bolivian high to the upper troposphere triggers the South American monsoon (Sarricolea and Romero 2015).

Changes in atmospheric circulation patterns modify precipitation patterns as well, contributing to irregularity in precipitation in this area. Some conclusive changes have been identified. A northward shift of the inter-tropical convergence zone (ITCZ) has been linked to changes in rainfall patterns in the Amazon basin (Schneider et al. 2014; Zappalá et al. 2018; Green et al. 2019). On a monthly scale, extreme events are linked to convection in the western Amazon basin during the wet season (Segura et al. 2019).

The wet season in northern Chile occurs in austral summer (between December and March). An increase in precipitation during this season is explained by an increase in vertical air instability and convection resulting from increased solar radiation and enhanced by topography (Junquas et al. 2016, 2018). At upper levels (250 to 200 hPa), the Bolivian High, related to the South American monsoon, introduces a humid easterly air mass from the Amazon Basin, which exhibits decadal and interdecadal variability (Segura et al. 2016, 2020; Vasconcellos et al. 2020).

In the south of the study area, precipitation is also influenced by westerly flows linked to cut-off low pressure configurations in the mid-troposphere (500 hPa, Garreaud 2009). Different mechanisms occur at different tropospheric levels, and changes in tropospheric circulation modify the trajectories of the air masses, originating precipitation.

There remain many questions regarding the mechanisms operating at different tropospheric levels, the origin of the air masses that produce rainfall events (especially extreme rainfall events), and the origin of moisture. This is important because water is a very scarce resource in northern Chile (Sarricolea et al. 2017b). Various factors, including mining urbanisation, have increased the demand for water based on the development strategy proposed by the country for the period 2017–2022 (Chilean Government 2015). However, this development strategy ignores potential future water supply problems, partly because precipitation projections can be misleading, exhibiting consistency at large spatial scales, but displaying significant uncertainty at local and regional scales (Power et al. 2012).

Factors causing extreme precipitation depend on physical parameters such as moisture availability, vertical stability, and event duration (Barlow et al. 2019). These factors in turn depend on mechanisms operating at different tropospheric levels and the origin of the air masses involved in such atmospheric processes (Chen and Zhai 2016). Meseguer-Ruiz et al. (2020) showed that daily precipitation anomalies in northern Chile were caused by changes in sea level pressure (slp) and geopotential height anomalies, but no research has been conducted regarding extreme precipitation.

The goals of this study were: 1) determine the origin of the air masses involved in daily extreme rainfall events (greater than 90th percentile of non-zero daily precipitation) in northern Chile, and consider the strength, direction, and vorticity of the flow at three different tropospheric levels (slp, 500 hPa and 250 hPa) and 2) identify dominant moisture sources and pathways for each coherent region defined by back trajectories for the summer season according to the HYSPLIT model.

The present study states as follows. Section 2 describes the dataset quality control, the cluster analysis carried out, the calculation of the strength, direction and vorticity of the flow, and the HYSPLIT set-up. Section 3 presents the main results of the study and their comparisons with other studies. Their discussion was drawn in section 4, along with the conclusions.

2. Data and methods

To accomplish our objectives, we first validated data quality. Next, we performed a cluster analysis to identify areas of homogeneity within the study area. Once this step was completed, we selected the closest meteorological station to each cluster centroid and determined the values of the independent variables required for JC classification: direction (D), strength (F), and vorticity (W) (Meseguer-Ruiz et al. 2019b). Back trajectories were obtained for each day of extreme precipitation (in the 90% percentile) and for each reference station using the HYSPLIT model (Stein et al. 2015).

2.1. Data quality

Daily rainfall records from 161 stations across the study area for the period 1 January 1966 to 31 December 2015 comprised the dataset Quality control was performed using Climatol version 3.0 package in R software (Guijarro 2016), which uses normal ratio values (data divided by the mean of its series) from the closest precipitation data to build reference series for all stations. Differences between the observed and reference series were used to test data quality by outlier detection, and their homogeneity was assessed using the Standard Normal Homogeneity Test (SNHT) (Alexandersson 1986). At the same time, undoing the normalisation of the reference series provides estimations to fill in missing data in the series. The monthly aggregates of the series allowed to detect significant shifts in the mean. For arid climates, daily series show a high degree of variability, so detection of variations in the mean is very difficult (Vincent et al. 2002). These data were previously used and results published in a related study (Meseguer-Ruiz et al. 2019a).

2.2. Cluster analysis

Cluster analysis using the k-means method of the data from 161 meteorological stations differentiated four distinct groups as a function of latitude, longitude, and accumulated rainfall, and the station closest to the centroid of each cluster was selected, one from each group. The decision to use four groups was based on the conclusions obtained in previous studies, and according to the altitude, latitude, terrain slope and orientation, distance to the Amazon Basin and concentration of the daily precipitation (Baltazar Fernandez and Meseguer-Ruiz 2019, Meseguer-Ruiz et al. 2019a).

To determine whether these groups depend on geographical location or on the amount of daily accumulated rainfall, the cluster analysis was reanalysed 1000 times by randomly rearranging accumulated rainfall values corresponding to each location while maintaining latitude and longitude. The resulting cluster assignments were compared with the original by summarising the agreement between groups by station and by cluster.

2.3. D, F and Z calculation

The JC method of classification (Jenkinson and Collison 1977) is an objective classification of weather types and one of the most popular methods used to link atmospheric circulation and precipitation. It is an automated method that determines the type of atmospheric circulation from atmospheric pressure reduced to sea level in a day and can be adapted to different tropospheric levels (Meseguer-Ruiz et al. 2019b; Miró et al. 2020). Due to its simplicity, this method has been applied in many regions worldwide (Casado and Pastor 2016; Putniković et al. 2016; Fealey and Mills 2018; Putniković and Tošić 2018). The JC classification system derives from the values of and relationships between flow strength (F), flow direction (D), and vorticity (Z). Because of its simplicity, the system is also well-suited to evaluate the representation of weather types over Europe in a suite of climate model simulations (Otero et al. 2018). The behaviour of these variables has been linked to variability in precipitation intensity, focusing on the circulation vorticity in high elevation areas, such as the Tibetan Plateau (Li et al. 2019).

The variables which to be determined are the zonal component of the geostrophic wind (W), the meridional component of the geostrophic wind (S), the wind direction (D) in azimuthal degrees, the wind speed (F) in m/s, the zonal component of vorticity (Zw), the meridional component of vorticity (Zs), and the total vorticity (Z). These values were calculated at three tropospheric levels: slp, 500, and 250 geopotential heights, according to a 9-point grid (Fig. 2). The atmospheric pressure and geopotential height data were obtained for the 1966–2015 NCEP/NCAR Reanalysis Project (Kalnay et al. 1996). The analytical expressions adjusted for northern Chile are as follows:

$$W = 0.25[(P1 + 2P2 + P3) - (P7 + 2P8 + P9] \quad (1)$$

$$S = 1{,}082[0.25(P1 + 2P4 + P7) - 0.25(P3 + 2P6 + P9)] \quad (2)$$

$$D = arctan\frac{W}{S} \quad (3)$$

$$F = \sqrt{\frac{W^2}{S^2}} \quad (4)$$

$$Z_W = 1.273[(P1 + 2P2 + P3) - (P4 + 2P5 + P6)] - 0.829[(P4 + 2P5 + P6) - (P7 + 2P8 + P9)] \quad (5)$$

$$Z_S = 0.830[0.25(P1 + 2P4 + P7) - 0.25(P2 + 2P5 + P8) - 0.25(P2 + 2P5 + P8) + 0.25(P3 + 2P6 + P9)] \quad (6)$$

$$Z = Z_W + Z_S \quad (7)$$

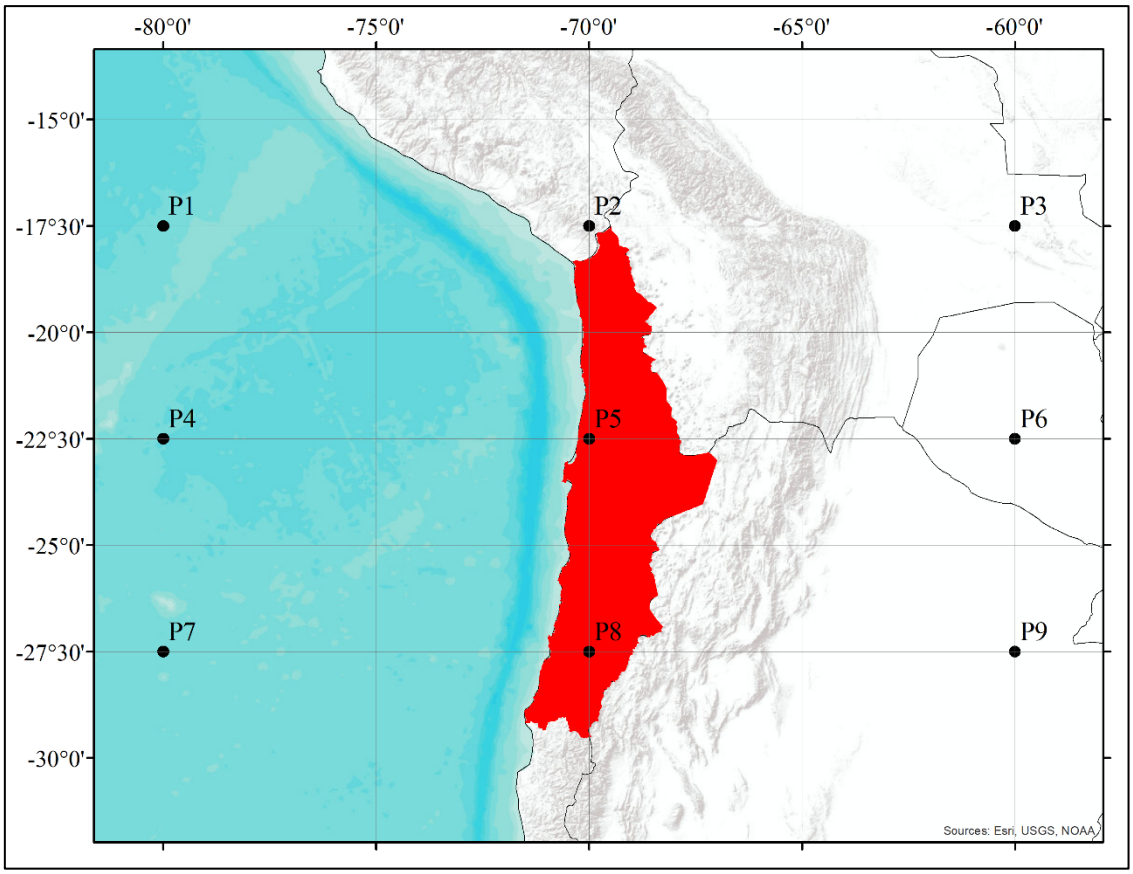

Figure 2. Location of the points used to determine the F, D and Z values.

First, we applied this methodology to obtain the behaviour of the independent variables (D, F, and Z) at three different tropospheric levels: SLP, 500 hPa, and 250 hPa. To calculate D, F, and Z at SLP, it is directly given by the above mentioned equations. For 500 hPa and 250 hPa levels, geopotential elevations were used. In this case, F and Z cannot be expressed in the same units or with the same range of magnitude as for the surface analysis because their calculation was based on geopotential height, but they do reference the above-ground flow behaviour, as shown in a study by Meseguer-Ruiz et al. (2019b). The selection of the JC classification method responds to its reliability determining the frequency behaviour of F, D and Z, and because it can be applied at different tropospheric levels and latitudes (Meseguer-Ruiz et al. 2019b).

2.4. Back trajectories

The HYSPLIT model from NOAA (Draxler and Hess 1998) allows computation of simple air particle trajectories as well as simulations of transport, dispersion, and deposition (Stein et al. 2015). The HYSPLIT model is one of the most widely used in atmospheric sciences to determine the origin of air masses and define the source-receptor linkage (Gustafsson et al. 2010; Fleming et al. 2012). The use of gridded climate data allows the HYSPLIT model to define a pathway for an air parcel arriving at a specific location at a given time on a particular date (Tan et al. 2018).

We used NOAA's HYSPLIT model to determine the back trajectories. Meteorological data were obtained from the NCEP/NCAR Reanalysis database with 2.5 degrees resolution. Due to the orographic complexity of the study area, the set-up of the model was based on mean sea level: 0 m at SLP, 5500 m at 500 hPa (to identify possible cut-off lows), and 12,000 m at 250 hPa (to identify the Bolivian High). With these settings, we obtained the back trajectories for 72 h, departing at 18:00 UTC-4 for each of the rainiest (90th percentile) days for the reference series of each cluster for the 1966–2015 period, following the methodologies applied by Gustafsson et al. (2010) and Bracken et al. (2015), but considering a 72 h pathway.

3. Results

3.1. Grouping based on the daily rainfall

A cluster analysis that accounted for the latitude and longitude of the stations and the mean annual accumulated rainfall was performed. This procedure used a multivariate analysis with the aim of differentiating the various observatories into groups with a high degree of external heterogeneity and internal homogeneity. The final centres of the three variables considered in each cluster are listed in Table

1. The differences between the factors considered in each cluster were significant (> 99%), which demonstrates external heterogeneity and internal homogeneity. The groupings are shown in Figure 3.

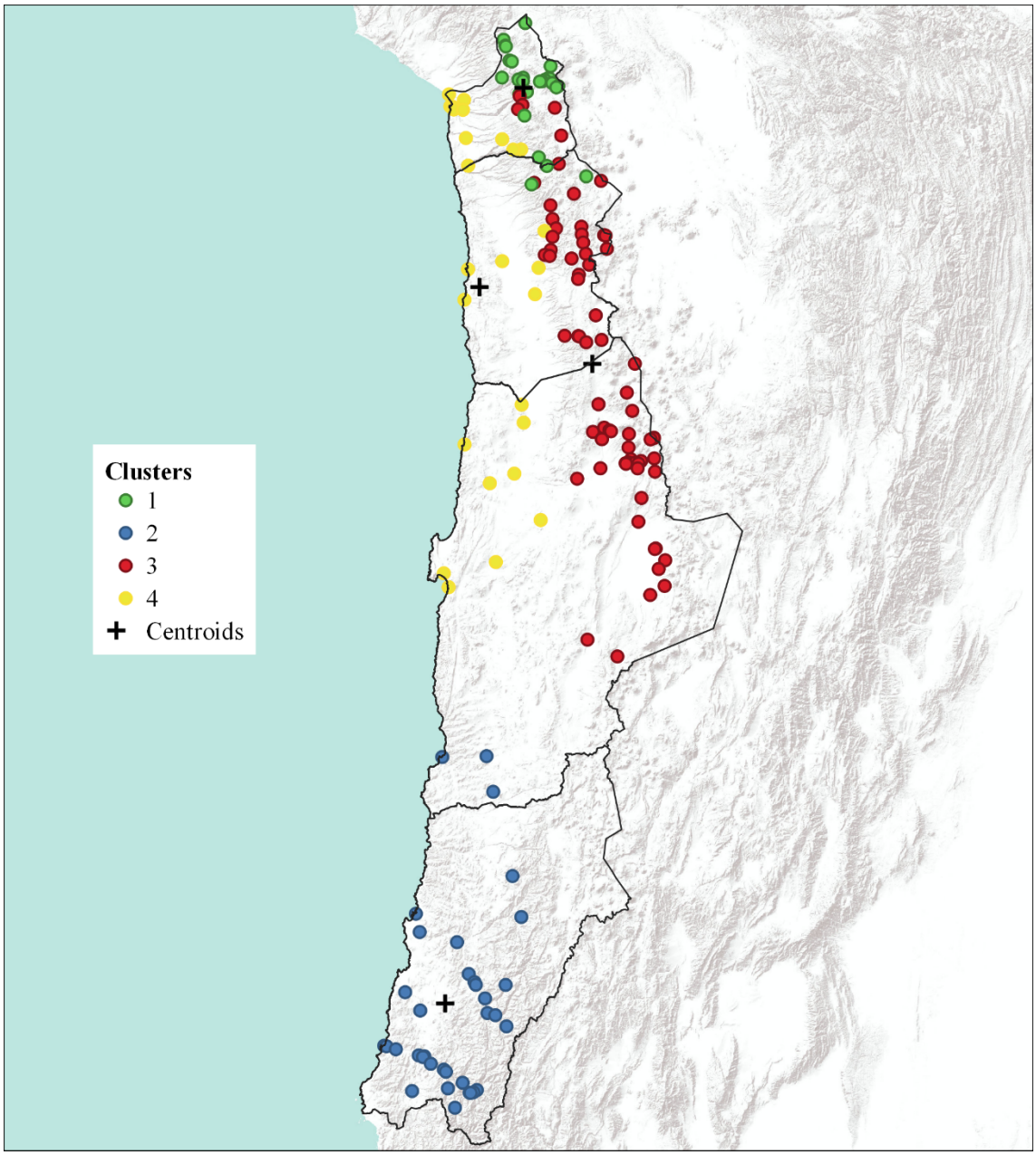

Figure 3. Stations grouping together after the cluster analysis

Table 1. Reference stations for each cluster (closest to the cluster's centroid).

Cluster	Station	Altitude (m a.s.l.)	Latitude (º S)	Longitude (º W)
1	Portezuelo Chapiquia	4,375	18.32	69.47
2	Los Loros	940	27.83	70.11
3	Ujina	4,300	20.97	68.63
4	Iquique	50	20.21	70.13

The next analysis was performed to confirm that geographical constraints were not the sole cause of the clusters obtained (Fig. 3), but clustering also depended on precipitation. After 1000 iterations to compute simulated clusters with randomly rearranged precipitation values, comparison with the original groups showed that the clusters were not the same in any simulation. The mean coincidence of each cluster group between the original and the iterated cluster analysis by station (Fig. 4) was less than 35%. When we

considered the percentage of stations that coincided with the original clusters (Fig. 5), the average of all of them is near zero. The iterated cluster analysis showed that the grouping was not solely geographic. Longitude and latitude could have influenced cluster 1, but not exclusively. Instead, clustering mainly depended on daily rainfall values. The observatories at Portezuelo Chapiquia, Los Loros, Ujina, and Iquique were selected as representative of clusters 1, 2, 3 and 4, respectively.

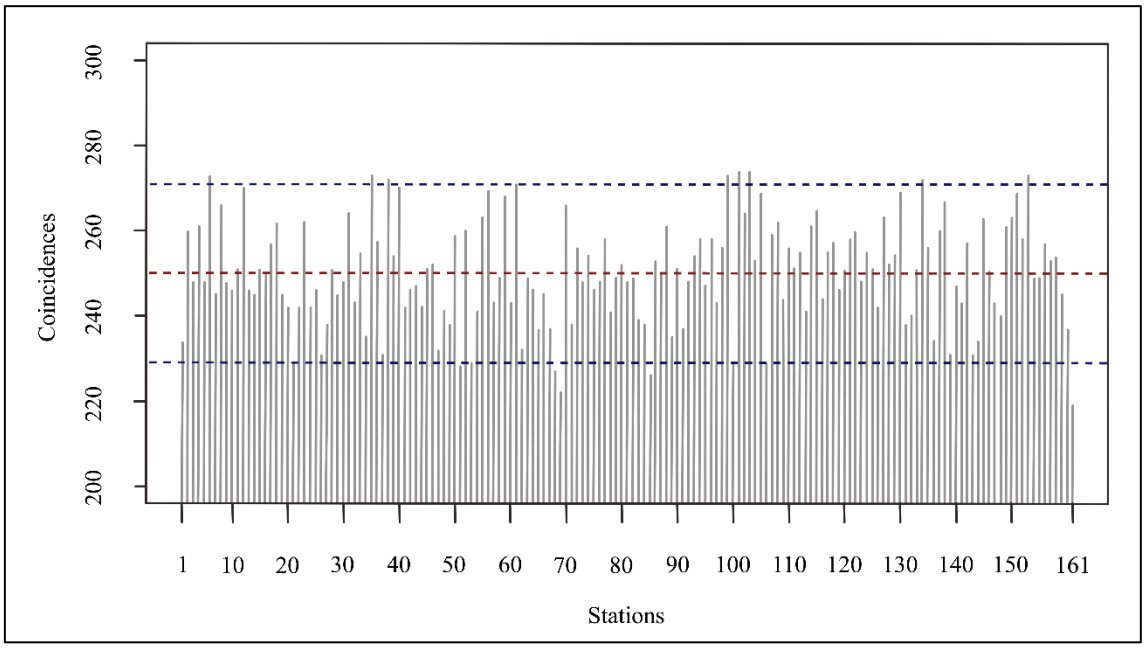

Figure 4. Number of cluster coincidences by stations between observed and simulated in the cluster analysis (grey bars) after 1,000 iterations. Red dashed line shows the mean number of coincidences and upper and lower dashed blue lines show the 95th and 5th percentile, respectively.

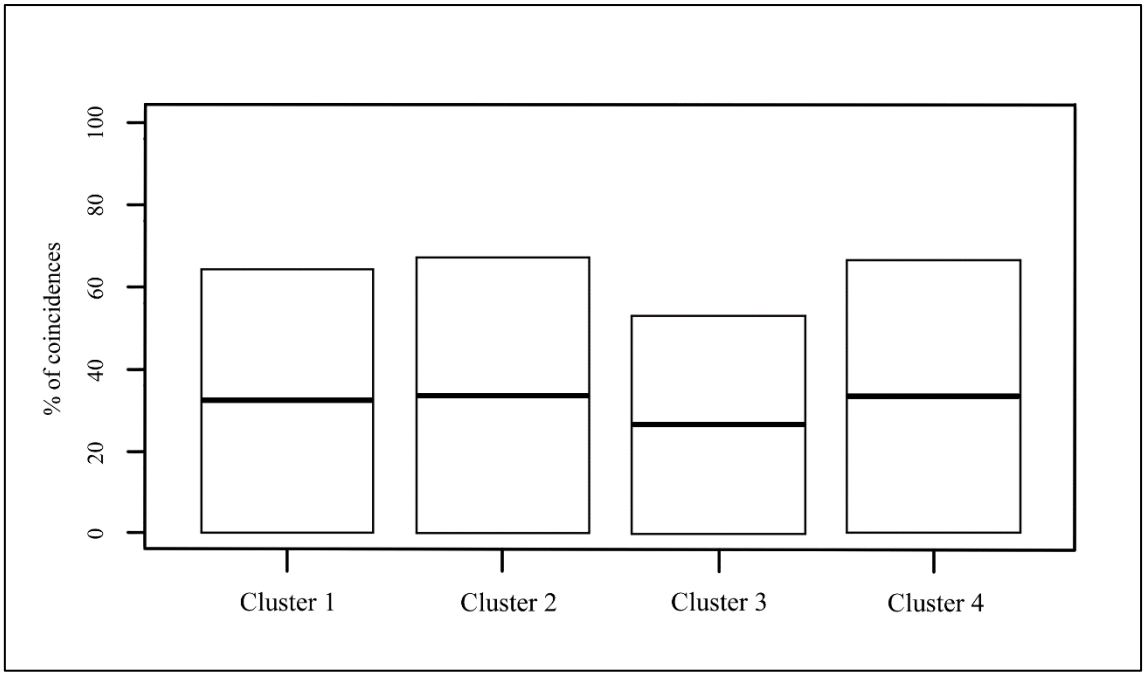

Figure 5. Boxplot of the percentage of coincident stations by clusters in the same analysis

3.2. D, F and Z frequency behaviour

The frequency of D, F, and Z was expressed as the kernel density for all the rainy days and for the extreme precipitation events for each cluster at each of three tropospheric levels (Fig. 6).

At slp, the most frequent D for rainy days in the period 1966–2015 had a southerly component. Flow F ranged from 6 to 8 m/s, and Z had frequent positive values that varied between 8 and 11 (black lines). Considering extreme precipitation events, cluster 1 showed a clear predominance of a southerly component

for D between 180º and 195º, and F values were approximately 6 m/s. Z values (always positive) were most frequent at 10 (green lines). Cluster 2 shows a high frequency at 200º, not centred at 180º, but with some cases at 25º and 130º, and a lower frequency for rainy days. F values exhibited a wide distribution from low flow strength (0 to 3 m/s) to high flow intensity (>15 m/s). The highest frequency for Z values was 10, but the important frequencies were negative values (from -10 to 0). Clusters 3 and 4 showed the same dominant southerly component, and flow strengths were most frequent for 7 and 7.5 m/s, respectively. The Z values for both clusters were almost always positive (with very few negative values), and more frequent for values around 13 in both cases.

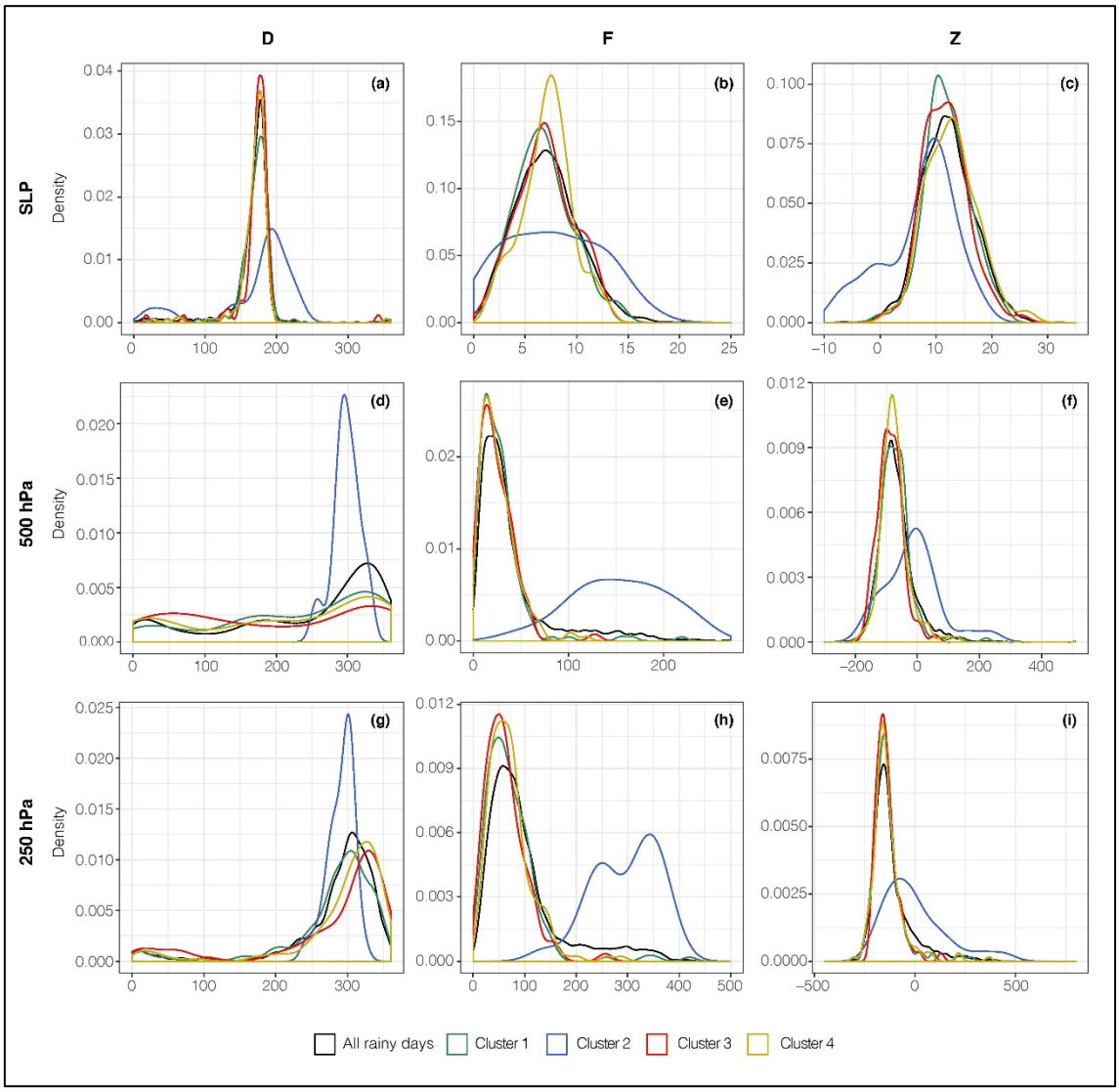

Figure 6. Variation of D, F and Z at slp, 500 hPa and 250 hPa for all the rainy days (black line) of the study period (1966-2015) and for the days of extreme precipitation in each cluster (coloured lines)

At 500 hPa, the most frequent flow direction was between 290º and 315º, F values were less than 50 m/s and Z values were slightly negative for rainy days. Meanwhile, cluster 1 showed a higher frequency with respect to D, ranging from 345º to 000º, as well as for clusters 3 and 4, but with some flows coming from all directions; while cluster 2 showed a clear predominance for a frequency centred around 300º. Regarding F, all the rainy days and clusters 1, 3, and 4 exhibited high frequencies for low F values. Cluster 2 showed a different behaviour for extreme precipitation events and all events with high F values. Regarding vorticity, for all the rainy days and in all the clusters, Z exhibited a negative behaviour. Cluster 2 showed the most frequent Z for null values but reached high positive values as well.

At 250 hPa, the reference period exhibited a clear component for D centred at 300º, F values were frequent in the range of 75 to 100 m/s, and Z values were frequently in the negative range. Cluster 1 showed a predominance for 300º, as well as cluster 3 and cluster 4, both of which centred around 315º. Cluster 2 also centred at 300º, and showed more affinity for this direction than the other clusters. Regarding F, all the

rainy days showed light strength, and the frequency increased for clusters 1, 3, and 4, all centred at 50º. Cluster 2 showed very high frequency for F, ranging between 200 and 400 m/s. The vorticity presented negative values in all cases, but rainy days and clusters 1, 3, and 4 showed some slightly positive cases, while cluster 2 showed fewer negative cases, but only a few positive and very positive ones.

3.3. Back trajectories analysis

At the surface level and for cluster 1 (Fig. 7a), the south-south-west component trajectories predominated, with those coming from the north-east appearing as the second most predominant component. Thus, a greater influence of flows from the Pacific than from the Amazon basin is highlighted. For cluster 2 (Fig. 7b), in addition to a fewer number of days of intense precipitation, it is also important to note that most of these days indicate a pathway from the north, and very few days with trajectories from other quadrants. Cluster 3 (Fig. 7c) shows a dominance of flows from the south-east, with a small number coming from the north-east from the Amazon basin and the Bolivian Altiplano. The same is true for cluster 4 (Fig. 7d), with a majority of trajectories marking a southerly component that eventually turns eastward. In this case, the trajectories coming from the Bolivian Altiplano are testimonial to their frequency. Summing up, in clusters 1, 3, and 4, the rainiest days have mainly southerly component trajectories at SLP; the opposite direction is true for cluster 2.

At 500 hPa, cluster 1 (Fig. 8a) shows a large number of trajectories coming from the Bolivian Altiplano, although they also come from the Pacific. At the same time, it is intuitive how the latter are affected by an anticyclonic turn and would describe a trajectory that intercepts the continental area. It is interesting to note that the two longest trajectories coming from the Pacific show a cyclonic turn.

Cluster 2 (Fig. 8b) shows how in the middle troposphere, intense precipitation occurs with predominately westerly flows, but with some flows coming from the north, although to a lesser extent. This cluster shows clear differences from the others when analysing the length of the described trajectories: the air mass that arrives at 18:00 UTC-4 on a day with extreme precipitation at the reference station in this cluster; 72 h earlier and far away (perhaps thousands of kilometres), over the Pacific Ocean. Cluster 3 (Fig. 8c) shows almost all the trajectories originating in the Bolivian Altiplano 72 h prior to extreme precipitation events in the Atacama Desert. The same is true for Cluster 4 (Fig. 8d), where a concentration of trajectories over the same area referred to for the previous cluster is evident, and in addition to a significant number of trajectories originated in the Amazon basin.

For the high troposphere (250 hPa) at cluster 1 (Fig. 9a), the back trajectories predominate over the Bolivian Altiplano, but this time they completely transcend the limits of that area and affect a large portion of the Amazon basin in northern Argentina, eastern Bolivia, western Paraguay, and Brazil. Trajectories originating in the Pacific Ocean and southern Peru also appear. For cluster 2 (Fig. 9b), all the back trajectories originated from the Pacific Ocean and have a westerly component. The case for clusters 3 (Fig. 9c) and 4 (Fig. 9d) is similar to that of cluster 1, with the trajectories predominately over Bolivia, but in both cases, transcending this boundary and affecting the Amazon basin and Pacific Ocean regions.

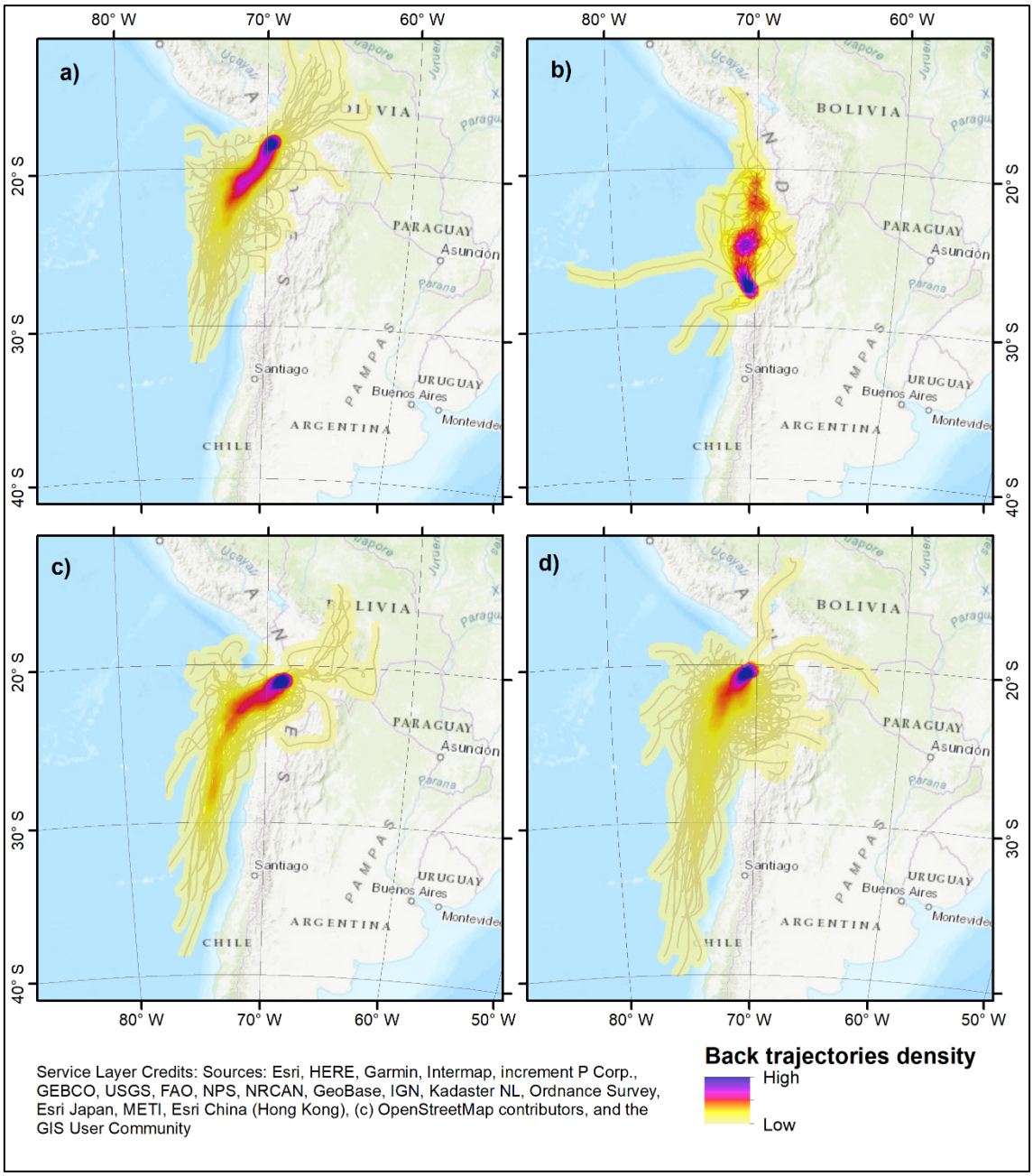

Figure 7. Back trajectories for each cluster for days with torrential rainfall at slp for a) cluster 1, b) cluster 2, c) cluster 3, and d) cluster 4

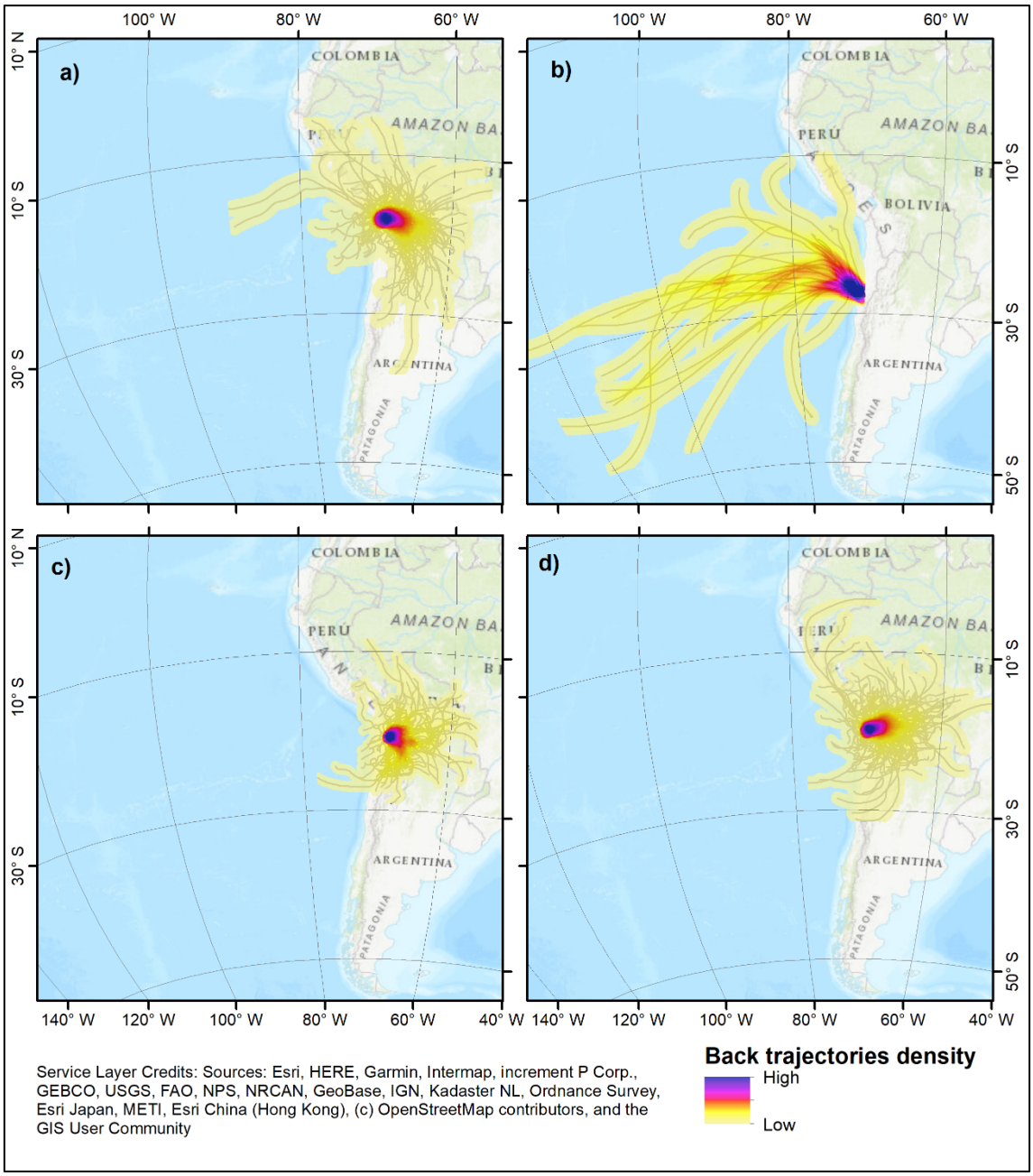

Figure 8. Back trajectories for each cluster for days with torrential rainfall at 500 hPa for a) cluster 1, b) cluster 2, c) cluster 3, and d) cluster 4

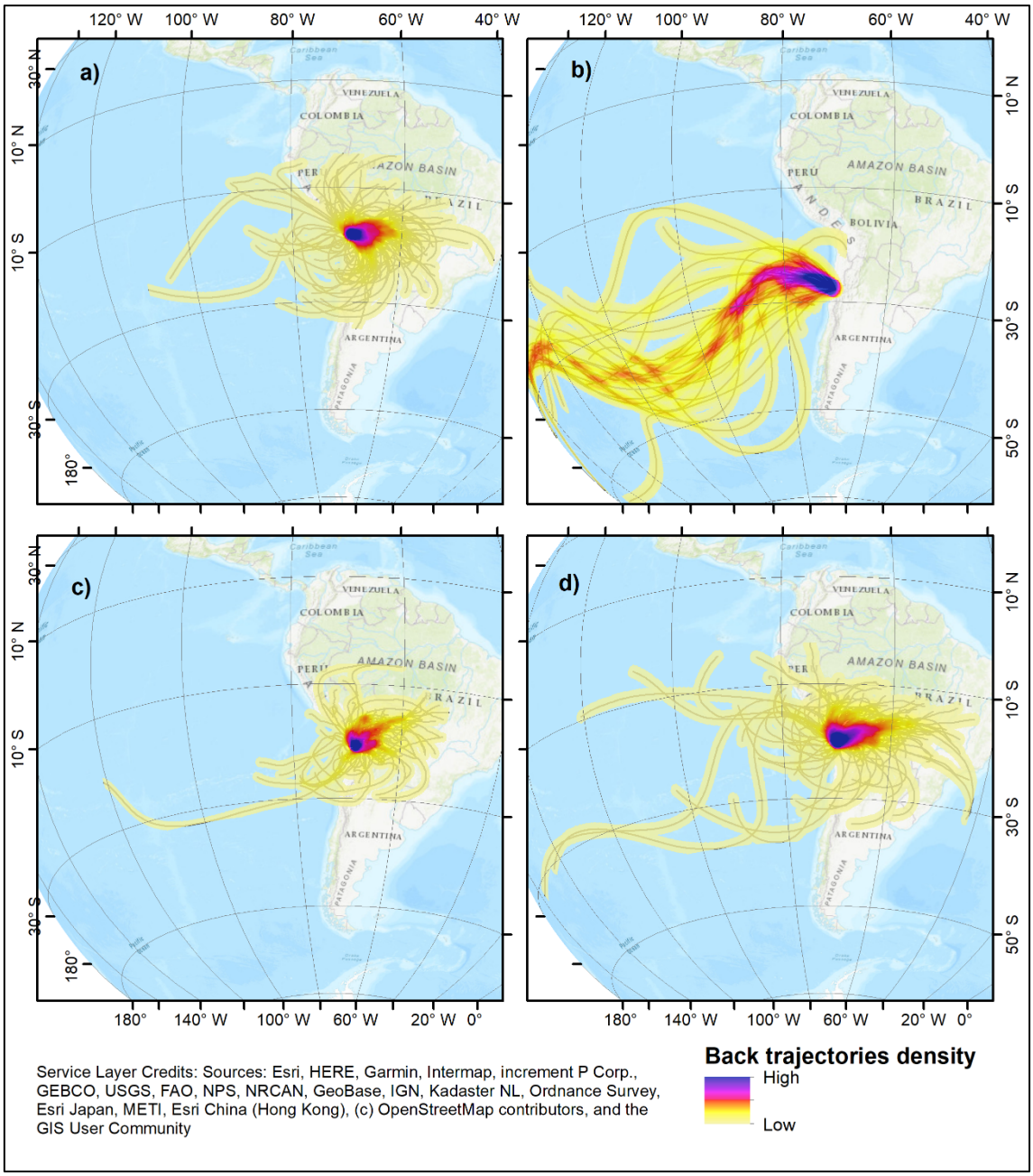

Figure 9. Back trajectories for each cluster for days with torrential rainfall at 250 hPa for a) cluster 1, b) cluster 2, c) cluster 3, and d) cluster 4

4. Discussion and conclusions

Regarding the behaviour of D, F, and Z, it is evident that the southern region of the study area (cluster 2) behaved differently from the other clusters. This could be related to the different processes taking place at this latitude, but also by the less frequent occurrence of extreme precipitation events registered for this region.

Vorticity exhibits a quite different behaviour compared to the mean values, so it appears as an important factor that modulates intense precipitation at different tropospheric levels (de Vries et al. 2018; Khansalari et al. 2020). All the clusters show higher vorticity values in cases of intense precipitation, and agreeing with the results presented by Li et al. (2019): more intense vorticity and flow intensity, associated water vapour transport, strong upper-level jet stream, and intense South Pacific high pressure, could contribute to intense precipitation, which in turn could be related to different flow directions. This is evident at 500 hPa, where for all clusters, except cluster 2, where torrential events came from all directions. This explains that the flow direction in the 24 h prior to an event is not that determinant on vorticity, but it is evident that the Pacific Ocean component plays a key role.

The analysis of the back trajectories at the different tropospheric levels identified behavioural similarities in clusters 1, 3, and 4, with cluster 2 presenting the greatest degree of difference with respect to the others, mainly due to the northerly component in D that occurs at the surface and the westerly component that occurs in the middle and upper troposphere. This agrees with the results presented in Baltazar Fernández and Meseguer-Ruiz (2019), where the daily precipitation concentration was much more reduced in this southern coastal region, and likely linked to the more frontal origin of precipitation. Meanwhile, for the rest of the study area, precipitation showed a convective origin. At these latitudes (25ºS), it is possible that cold fronts coming from the Pacific Ocean arrive and cause frontal precipitation to occur.

At the surface level, the fact that torrential rainfall caused by flows of oceanic origin is related to the possible configuration of surface low pressures off the coast of northern Chile that encourage flow of southerly and then westerly components that provide moisture to the continent (Sarricolea and Romero 2015). Colliding with the abrupt coastal relief and steep sections of the Andes Mountains, these easterly flows are forced to ascend rapidly causing precipitation (Junquas et al. 2016, 2018). This phenomenon responds to processes of a synoptic scale, coinciding with what was indicated in previous studies (Junquas et al. 2016, 2018; Barlow et al. 2019; Meseguer-Ruiz et al. 2020), or local processes derived from thermal differences between the continent and the ocean.

In the middle and upper troposphere, the trajectories show an evident origin in the Bolivian Altiplano, which highlights the influence that relief plays in the configuration of the so-called Bolivian High (Segura et al. 2016, 2018) and the northward extension of the low level jet stream (Segura et al. 2019), introducing humid air flow from the Amazon basin that interacts directly with the South American monsoon (Sarricolea and Romero 2015; Meseguer-Ruiz et al. 2019a). First, this shows the importance of this summertime pattern in the region (Marengo et al. 2012).

Nevertheless, changes in this system in recent years and those expected in the future (Jones and Carvalho 2013) suggest a lesser influence on precipitation as noted in Segura et al. (2020). The results described in Segura et al. (2019) suggest that in the northern part of the study area, extremely rainy seasons are linked to sea surface temperature anomalies in the central equatorial Pacific, but none of the pathways analysed here allowed us to confirm this statement.

The extreme precipitation events can also be linked to the Madden-Julian Oscillation (MJO) which propagates anomalies in convection and circulation, with a key role played by the orography in the study area (Grimm 2019) and agree with the results presented here. In a warmer climate, uncertainties arise concerning this point because MJO-related precipitation can increase intensity and affect wind in these regions (Maloney et al. 2019). This phenomenon could be related to changes in the pathways and in the D, F, and Z at different tropospheric levels that could help to improve predictions of extreme weather in this region. It is well known that synoptic circulation is better represented by simulation than precipitation. The mechanisms of tropical-extratropical interactions leading to the occurrence of extreme precipitation are explained by a vorticity intrusion forcing the incursion of tropical water vapour, in agreement with the findings of de Vries et al. (2018) for another arid subtropical region.

Torrential rainfall in cluster 2 could be associated with the configuration of cut-off low pressure systems in front of the continent that would have their evidence in the middle troposphere and would provide flows of oceanic origin, coinciding with what was proposed by Garreaud (2009) and demonstrated in a study by Meseguer-Ruiz et al. (2020). These results show that extreme precipitation over northern Chile mainly results from the effects of synoptic scale in the north, and large-scale atmospheric circulation in the southern coastal region. This also agrees with the results presented by Segura et al. (2020), who stated that easterly circulation in upper levels no longer correlates with precipitation, and suggests that this region may have experienced a change in the dominant mode of atmospheric circulation.

Different regions across northern Chile show distinct patterns of pathways in timing for 24 h of extreme precipitation, but it is difficult to make a statement about which processes explain the gain of specific humidity from the present pathway analysis due to differences in criteria when considering the origin time of the different pathways as compared to other similar studies (Gustafsson et al. 2010, Bracken et al. 2015), in which times varied from 15 to 32 h. Thus, consideration of the lag time from the initial conditions that eventually produced the extreme precipitation event is highly relevant to determine the pathway followed by the relevant air masses.

Acknowledgments

The authors want to thank the FONDECYT Project 11160059 of the Chilean Government, the Climatology Group (2017SGR1362, Catalan Government) and the CLICES Project (CGL2017-83866-C3-2-R) for the institutional support. R.S.N. is funded by the Spanish Ministry of Science and Innovation (grant no. FJCI-2017-31595).

References

Alexandersson H (1986) A homogeneity test applied to precipitation data. Int J Climatol 6:661-675. https://doi.org/10.1002/joc.3370060607
Baez-Villanueva OM, Zambrano-Bigiarini M, Ribbe L, Nauditt A, Giraldo-Osorio JD, Thinh NX. (2018) Temporal and spatial evaluation of satellite rainfall estimates over different regions in Latin-America. Atmos Res 213:34-50. https://doi.org/10.1016/j.atmosres.2018.05.011
Baltazar Fernández A, Meseguer-Ruiz O (2019) Regionalization of the Concentration Index in northern Chile and its relation with the orographic component (1966-2015). Investigaciones Geográficas, 57:32-48. https://doi.org/10.5354/0719-5370.2019.53440
Barlow M, Gutowski Jr WJ, Gyakum JR, Katz RW, Lim YK, Schumacher RS, Wehner MF, Agel L, Bosilovich M, Collow A, Gershunov A, Grotjahn R, Leung R, Milrad S, Min SK. (2019) North American extreme precipitation events and related large-scale meteorological patterns: a review of statistical methods, dynamics, modeling, and trends. Clim Dyn 53:6835-6875. https://doi.org/10.1007/s00382-019-04958-z
Bombi P. (2018) Potential impacts of climate change on Welwitschia mirabilis populations in the Namib Desert, southern Africa. J Arid Land 10:663-672. https://doi.org/10.1007/s40333-018-0067-1
Bracken C, Rajagopalan B, Alexander M, Gangopadhyay S. (2015) Spatial variability of seasonal extreme precipitation in the western United States. J Geophys Res Atmos 120:4522-4533. https://doi.org/10.1002/2015JD023205
Casado MJ, Pastor MA. (2016) Circulation types and winter precipitation in Spain. Int J Climatol 36:2727-2742. https://doi.org/10.1002/joc.3860
Castino F, Bookhagen B, Strecker MR. (2017) Rainfall variability and trends of the past six decades (1950–2014) in the subtropical NW Argentine Andes. Clim Dyn 48: 1049-1067. https://doi.org/10.1007/s00382-016-3127-2
Chen Y, Zhai P. (2016) Mechanisms for concurrent low-latitude circulation anomalies responsible for persistent extreme precipitation in the Yangtze River Valley. Clim Dyn 47:989-1006. https://doi.org/10.1007/s00382-015-2885-6
Chilean Government (2015) Plan de Adaptación al Cambio Climático. Departamento de Cambio Climático del Ministerio del Medio Ambiente, Santiago.
De Vries AJ, Ouwersloot HG, Feldstein SB, Riemer M, El Kenawy AM, McCabe MF, Lelieveld J. (2018) Identification of Tropical-Extratropical Interactions and Extreme Precipitation Events in the Middle East Based On Potential Vorticity and Moisture Transport. J Geophys Res Atmos 123:861-881. https://doi.org/10.1002/2017JD027587
Donat M, Lowry A, Alexander L, O'Gorman P, Maher N. (2016) More extreme precipitation in the world's dry and wet regions. Nat Clim Change 6:508-513. https://doi.org/10.1038/NCLIMATE2941
Draxler RR, Hess GD. (1998) An overview of the HYSPLIT_4 modeling system for trajectories, dispersion, and deposition. Aust Meteor Mag 47:295-308. Geophys Res Atmos 123:861-881. https://doi.org/10.1002/2017JD027587
Falvey M, Garreaud R. (2005) Moisture variability over the South American Altiplano during the South American low level jet experiment (SALLJEX) observing season. J Geophys Res 110:D22105. https://doi.org/10.1029/2005JD00615
Fealey R, Mills G. (2018) Deriving Lamb weather types suited to regional climate studies: A case study on the synoptic origins of precipitation over Ireland. Int J Climatol 38:3439-3448. https://doi.org/10.1002/joc.5495
Fleming ZL, Monks PS, Manning AJ. (2012) Review: Untangling the influence of air-mass history in interpreting observed atmospheric composition. Atmos Res 104-105:1-39. https://doi.org/10.1016/j.atmosres.2011.09.009
Garreaud RD. (2009) The Andes climate and weather. Adv Geosci 22:3–11. https://doi.org/10.5194/adgeo-22-3-2009
Garreaud R, Aceituno P. (2001) Interannual rainfall variability over the South American Altiplano. J Clim 14:2779–2789. https://doi.org/10.1175/1520-0442(2001)014<2779:IRVOTS>2.0.CO;2
Green B, Marshall J, Campin JM. (2019) The 'sticky' ITCZ: ocean-moderated ITCZ shifts. Clim Dyn 53:1-19. https://doi.org/10.1007/s00382-019-04623-5
Grimm AM. (2019) Madden–Julian Oscillation impacts on South American summer monsoon season: precipitation anomalies, extreme events, teleconnections, and role in the MJO cycle. Clim Dyn 53:907-932. https://doi.org/10.1007/s00382-019-04622-6
Guijarro JA (2016) Package "climatol" Climate Tools (Series Homogenization and Derived Products). https://CRAN.R-project.org/package=climatol
Gustafsson M, Rayner D, Chen D. (2010) Extreme rainfall events in southern Sweden: where does the moisture come from? Tellus A 62(5):605-616. https://doi.org/10.1111/j.1600-0870.2010.00456.x

476 Houston J, Hartley AJ. (2003) The central Andean west-slope rainshadow and its potential contribution to
477 the origin of hyper-aridity in the Atacama Desert. Int J Climatol 23:1453–1464.
478 https://doi.org/10.1002/joc.938
479 Insel N, Poulsen CJ, Ehlers TA. (2010) Influence of the Andes Mountains on South American moisture
480 transport, convection, and precipitation, Clim Dyn 35:1477-1492. https://doi.org/10.1007/s00382-009-
481 0637-1
482 Jenkinson AF, Collison P. (1977) An initial climatology of gales over the North Sea. Synoptic Climatology
483 Branch Memorandum no 62, Bracknell. Meteorological Office, London
484 Jones C, Carvalho LMV. (2013) Climate Change in the South American Monsoon System: Present Climate
485 and CMIP5 Projections. J Climate 26:6660-6678. https://doi.org/10.1175/JCLI-D-12-00412.1
486 Junquas C, Li L, Vera CS, Le Treut H, Takahashi K. (2016) Influence of South America orography on
487 summertime precipitation in Southeastern South America. Clim Dyn 46:3941-3963.
488 https://doi.org/10.1007/s00382-015-2814-8
489 Junquas C, Takahashi K, Condom T, Espinoza JC, Chavez S, Sicart JE, Lebel T. (2018) Understanding the
490 influence of orography on the precipitation diurnal cycle and the associated atmospheric processes in the
491 central Andes. Clim Dyn 50:3995-4017. https://doi.org/10.1007/s00382-017-3858-8
492 Kalnay E, Kanamitsu M, Kistler R, Collins W, Deaven D, Gandin L, Iredell M, Saha S, White G, Woollen
493 J, Zhu Y, Chelliah M, Ebisuzaki W, Higgins W, Janowiak J, Mo KC, Ropelewski C, Wang J, Leetmaa A,
494 Reynolds R, Jenne R, Joseph D (1996) The NCEP/NCAR 40-year reanalysis project. Bull Amer Meteor
495 Soc 77:437-470. https://doi.org/10.1175/1520-0477(1996)077%3C0437:TNYRP%3E2.0.CO;2
496 Khansalari S, Mohebalhojeh AR, Ahmadi-Givi F, Sprenger M. (2020) On the determining factors in cases
497 of moderate to heavy precipitation in Tehran. Theor Appl Climatol 140:1107-1123.
498 https://doi.org/10.1007/s00704-020-03133-3
499 Kirtman B, Power SB, Adedoyin JA, Boer GJ, Bojariu R, Camilloni I, Doblas-Reyes FJ, Fiore AM, Kimoto
500 M, Meehl GA, Prather M, Sarr A, Schär C, Sutton R, van Oldenborgh GJ, Vecchi G, Wang HJ. (2013)
501 Near-term climate change: projections and predictability. In Stocker TF, Qin D, Plattner GK, Tignor M,
502 Allen SK, Boschung J, Nauels A, Xia Y, Bex V, Midgley PM. (Eds.) Climate Change 2013: The Physical
503 Science Basis. Contribution of Working Group I to the Fifth Assessment Report of the Intergovernmental
504 Panel on Climate Change. Cambridge: Cambridge University Press, 953-1028
505 Kock ST, Schittek K, Mächtle B, Maldonado A, Vos H, Lupo LC, Kulemeter JJ, Wissel H, Schäbitz F,
506 Lücke A. (2020) Multi-centennial-scale variations of South American summer monsoon intensity in the
507 southern central Andes (24-27°S) during the late Holocene. Geophys Res Lett 47:e2019GL084157.
508 https://doi.org/10.1029/2019GL084157
509 Li L, Zhang R, Wen M, Duan J, Qi Y. (2019) Characteristics of the Tibetan Plateau vortices and the related
510 large-scale circulations causing different precipitation intensity. Theor Appl Climatol 138:849-860.
511 https://doi.org/10.1007/s00704-019-02870-4
512 Maloney ED, Adames AF, Bui HX. (2019) Madden–Julian oscillation changes under anthropogenic
513 warming. Nature Clim Change 9:26-33. https://doi.org/10.1038/s41558-018-0331-6
514 Marengo JA, Liebmann B, Grimm AM, Misra V, Silva Dias PL, Cavalcanti IFA, Carvalho LMV, Berbery
515 EH, Ambrizzi T, Vera CS, Saulo AC, Nogues-Paegle J, Zipser E, Seth A, Alves LM. (2012) Recent
516 developments on the South American monsoon system. Int J Climatol 32:1-21.
517 https://doi.org/10.1002/joc.2254
518 Marjani S, Alizadeh.Choobari O, Irannejad P. (2019) Frequency of extreme El Niño and La Niña events
519 under global warming. Clim Dyn. https://doi.org/10.1007/s00382-019-04902-1
520 Meseguer-Ruiz O, Ponce-Philimon PI, Guijarro JA, Sarricolea P. (2019a) Spatial distribution and trends of
521 different precipitation variability indices based on daily data in Northern Chile between 1966 and 2015. Int
522 J Climatol 39:4595-4610. https://doi.org/10.1002/joc.6089
523 Meseguer-Ruiz O, Osborn TJ, Sarricolea P, Jones PD, Olcina J, Serrano-Notivoli R, Martín-Vide J. (2019b)
524 Definition of a temporal distribution index for high temporal resolution precipitation data over Peninsular
525 Spain and the Balearic Islands: the fractal dimension; and its synoptic implications. Clim Dyn 52:439-456.
526 https://doi.org/10.1007/s00382-018-4159-6
527 Meseguer-Ruiz O, Cortesi N, Guijarro JA, Sarricolea P. (2020) Weather regimes linked to daily
528 precipitation anomalies in Northern Chile. Atmos Res 236: 104802.
529 https://doi.org/10.1016/j.atmosres.2019.104802
530 Miró JR, Pepin N, Peña JC, Martin-Vide J. (2020) Daily atmospheric circulation patterns for Catalonia
531 (northeast Iberian Peninsula) using a modified version of Jenkinson and Collison method. Atmos Res
532 231:104674. https://doi.org/10.1016/j.atmosres.2019.104674
533 Otero N, Sillmann J, Butler T. (2018) Assessment of an extended version of the Jenkinson–Collison
534 classification on CMIP5 models over Europe. Clim Dyn 50: 1559-1579. https://doi.org/10.1007/s00382-
535 017-3705-y

Pliscoff P, Luebert F, Hilger HH, Guisan A. (2014) Effects of alternative sets of climatic predictors on species distribution models and associated estimates of extinction risk: A test with plants in an arid environment. Ecol Model 288:166-177. https://doi.org/10.1016/j.ecolmodel.2014.06.003
Power SB, Delage F, Colman R, Moise A. (2012) Consensus on 21st century rainfall projections in climate models more widespread than previously thought. J Clim 25:3792-3809. https://doi.org/10.1175/JCLI-D-11-00354.1
Putniković S, Tošić I, Durdević V. (2016) Circulation weather types and their influence on precipitation in Serbia. Meteorol Atmos Phys 128:649-662. https://doi.org/10.1007/s00703-016-0432-6
Putniković S, Tošić I. (2018) Relationship between atmospheric circulation weather types and seasonal precipitation in Serbia. Meteorol Atmos Phys 130:393-403. https://doi.org/10.1007/s00703-017-0524-y
Rohde RF, Hoffman MT, Durbach I, Venter Z, Jack S. (2019) Vegetation and climate change in the Pro-Namib and Namib Desert based on repeat photography: Insights into climate trends. J Arid Environ 165:119-131. https://doi.org/10.1016/j.jaridenv.2019.01.007
Sarricolea P, Romero H. (2015) Variabilidad y cambios climáticos observados y esperados en el Altiplano del norte de Chile. Rev Geogr Norte Gd 62:169-183. https://doi.org/10.4067/S0718-34022015000300010
Sarricolea P, Herrera-Ossandon MJ, Meseguer-Ruiz O. (2017a) Climatic regionalisation of continental Chile. J Maps 13(2):66–73. https://doi.org/10.1080/17445647.2016.1259592
Sarricolea P, Meseguer-Ruiz O, Romero Aravena H. (2017b) Tendencias de la precipitación en el Norte Grande de Chile y su relación con las proyecciones de cambio climático. Diálogo Andino, Revista de Historia, Geografía y Cultura Andina 54:41–50. https://doi.org/10.4067/S0719-26812017000300041
Schneider T, Bischoff T, Haug GH. (2014) Migrations and dynamics of the intertropical convergence zone. Nature 513:45-53. https://doi.org/10.1038/nature13636
Segura H, Espinoza JC, Junquas C, Takahashi K. (2016) Evidencing decadal and interdecadal hydroclimatic variability over the Central Andes. Env Res Let 11:094016. https://doi.org/10.1088/1748-9326/11/9/094016
Segura H, Junquas C, Espinoza JC, Vuille M, Jauregui YR, Rabatel A, Condom T, Lebel T. (2019) New insights into the rainfall variability in the tropical Andes on seasonal and interannual time scales. Clim Dyn 53:405-426. https://doi.org/10.1007/s00382-018-4590-8
Segura H, Espinoza JC, Junquas C, Lebel T, Vuille M, Garreaud R. (2020) Recent changes in the precipitation-driving processes over the southern tropical Andes/western Amazon. 54:2613-2631. https://doi.org/10.1007/s00382-020-05132-6
Shukla PR, Skea J, Slade R, van Diemen R, Haughey E, Malley J, Pathak M, Portugal Pereira J. (2019) Technical Summary. In Shukla PR, Skea J, Calvo Buendia E, Masson-Delmotte V, Pörtner HO, Roberts DC, Zhai P, Slade R, Connors S, van Diemen R, Ferrat M, Haughey E, Luz S, Neogi S, Pathak M, Petzold J, Portugal Pereira J, Vyas P, Huntley E, Kissick K, Belkacemi M, Malley J. (eds.) Climate Change and Land: an IPCC special report on climate change, desertification, land degradation, sustainable land management, food security, and greenhouse gas uxes in terrestrial ecosystems. In press.
Stein AF, Draxler RR, Rolph GD, Stunder BJB, Cohen MD (2015) NOAA's HYSPLIT Atmospheric Transport and Dispersion Modeling System. B Am Meteorol Soc 96:2059-2077. https://doi.org/10.1175/BAMS-D-14-00110.1
Tan X, Gan TY, Chen YD. (2018) Moisture sources and pathways associated with the spatial variability of seasonal extreme precipitation over Canada. Clim Dyn 50:629-640. https://doi.org/10.1007/s00382-017-3630-0
Valdés-Pineda R, Valdés JB, Diaz HF, Pizarro-Tapia R. (2015) Analysis of spatio-temporal changes in annual and seasonal precipitation variability in South America-Chile and related ocean-atmosphere circulation patterns. Int J Climatol 36:2979–3001. https://doi.org/10.1002/joc.4532
Valdés-Pineda R, Cañón J, Valdés JB. (2018) Multi-decadal 40-to 60-year cycles of precipitation variability in Chile (South America) and their relationship to the AMO and PDO signals. J Hydrol 556:1153–1170. https://doi.org/10.1016/j.jhydrol.2017.01.031
Vasconcellos FC, Deng Y, Zhang H, Martins G. (2020) Austral summer precipitation biases over tropical South America in five CMIP5 earth system models. Int J Climatol. https://doi.org/10.1002/joc.6595
Vincent LA, Zhang X, Bonsal BR, Hogg WD (2002) Homogenization of daily temperatures over Canada. J Clim 15:1322-1334. https://doi.org/10.1175/1520-0442(2002)015<1322:HODTOC>2.0.CO;2
Williams CJR. (2017) Climate change in Chile: an analysis of state-of-the-art observations, satellite-derived estimates and climate model simulations. Journal of Earth Science & Climatic Change 8:5. https://doi.org/10.4172/2157-7617.1000400
Zappalà DA, Barreiro M, Masoller, C. (2018) Quantifying changes in spatial patterns of surface air temperature dynamics over several decades. Earth Syst Dynam 9:383-391. https://doi.org/10.5194/esd-9-383-2018